出國報告（出國類別：開會）

參加國際腫瘤外科學會(Society of Surgical Oncology, SSO) 2026 年會會議並代表台灣乳房醫學會(TBCS)擔任 SSO-TBCS 業務會議主持人

服務機關：臺北榮民總醫院外科部乳房外科
姓名職稱：黃其晟主治醫師兼科主任
派赴國家/地區：美國亞利桑那州鳳凰城
出國期間：115/3/4~115/3/9
報告日期：115/3/14

摘要

TBCS 與 SSO 於 2025 年簽訂 MOU，TBCS 也於 2023 年與 2024 年台北國際乳癌研討會(TIBCS 2023/2024)邀請並補助 SSO 代表與會交流。本次會議為 TBCS-SSO 簽訂 MOU 後首次由黃其晟醫師同時為 TBCS 秘書長現場參與 SSO 年會，基於對等互惠原則由 SSO 邀請參加與會。黃其晟醫師目前擔任 TBCS 秘書長並獲 SSO 邀請擔任 SSO- TBCS 業務會議主持人，此次會議有助於本國與全球共計 69 國腫瘤外科專科醫師與兩專業學會之交流。會議內容包含兩會年會互訪並進行業務會議，及年輕醫師辯論與短期醫院參訪等實質國際合作教流，並邀對方參與本國今年之 TIBCS 2026 會議。

關鍵詞：國際腫瘤外科學會(Society of Surgical Oncology, SSO)、台灣乳房醫學會(TBCS)、業務會議、空間體定序、乳小葉乳癌

目次

一、目的 5

二、過程 5

三、心得及建議 7

四、附錄 8

目的

外科部乳房外科黃其晟醫師(以下簡稱本人)獲國際腫瘤外科學會(Society of Surgical Oncology, SSO)邀請並補助至美國亞利桑那州鳳凰城參加 SSO 2026 年會會議，會議期間 115 年 3 月 5 日至 7 日，並擔任 SSO-台灣乳房醫學會(Taiwan Breast Cancer Society, TBCS)業務會議主持人。

TBCS 與 SSO 於 2025 年簽訂 MOU，TBCS 也於 2023 年與 2024 年台北國際乳癌研討會(TIBCS 2023/2024)邀請並補助 SSO 代表與會交流。本次會議為 TBCS-SSO 簽訂 MOU 後首次由本人同時為 TBCS 秘書長現場參與 SSO 年會，基於對等互惠原則由 SSO 邀請參加與會。此次會議有助於本國與全球共計 69 國腫瘤外科專科醫師與兩專業學會之交流。會議內容包含兩會年會互訪並進行業務會議，及年輕醫師辯論與短期醫院參訪等實質國際合作教流，並邀對方參與本國今年之 TIBCS 2026 會議。此外也應 SSO 邀請發表口頭論文一篇，並同時完成 Annals of Surgical Oncology (SSO 官方期刊)投稿(如附件)。

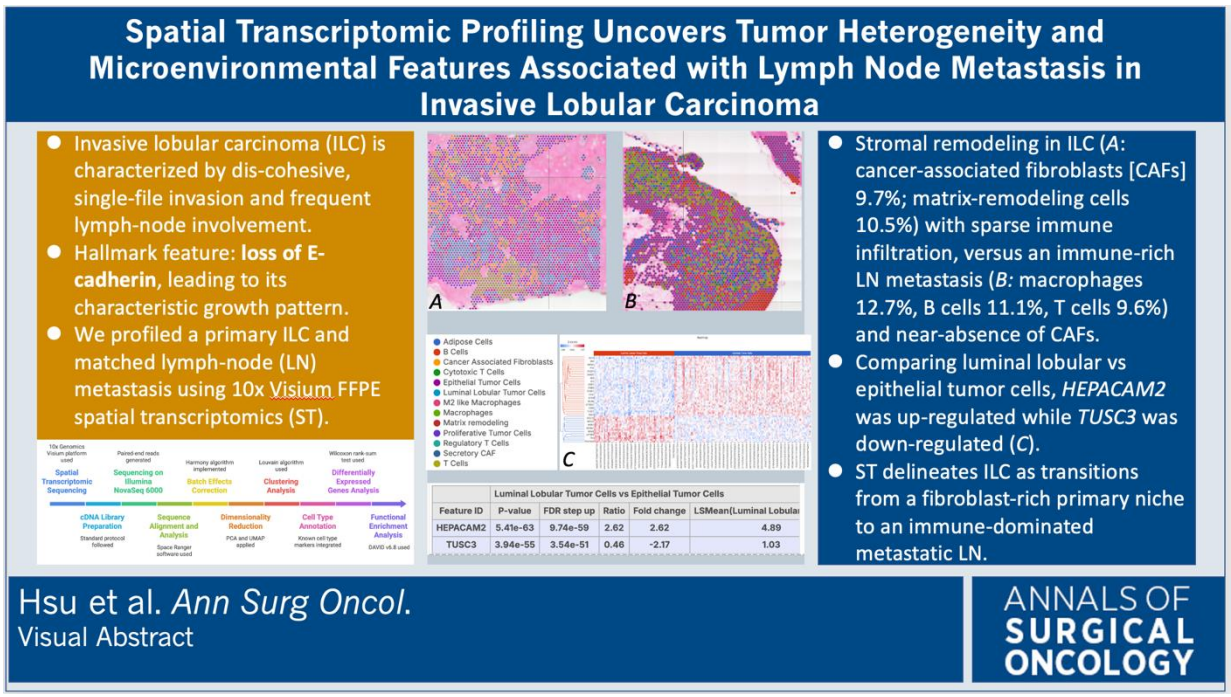

(ASO 投稿 Visual abstract)

過程

重點日程：

3/4（三）晚間：Welcome Reception、SSO President's Dinner (The El Chorro Lodge)

3/5（四）：Global Partner Abstract Program 口頭發表、Global Partner Leadership Summit
3/6（五）：Women in Cancer Surgery 等學術與社群活動
3/7（六）：Bilateral Meeting

口頭論文發表題目：Preliminary Spatial Transcriptomic Analysis for Invasive Lobular Carcinoma

本研究針對侵襲性小葉型乳癌（Invasive Lobular Carcinoma）進行初步空間轉錄體分析，探討腫瘤內不同微環境之分子表現差異與臨床決策之意涵。發表後與會者就技術流程、病例選取與臨床導入可行性進行熱絡討論，獲得正向回饋。Global Partner Abstracts 計畫係 SSO 提供予 15 個全球夥伴學會之專屬投稿與展示機制，並於年會當日安排 1 位口頭發表與 10 位海報展示；所有論文將刊登於 Annals of Surgical Oncology 增刊。

Global Partner Leadership Summit

Global Partner Leadership Summit 為 SSO 年會期間之高層級國際夥伴會議，對象為各國外科腫瘤相關學會（Global Partner Societies）之領導與國際事務代表；目的在於就學術研究、教育訓練、學術出版與國際合作等議題進行策略交流與共識凝聚。此活動採受邀制。由 SSO 領導團隊主持；Global Partner 列席包含 AORTIC、BSSO、COSECSA、EGSSO、ESSO、IASO、ISSO、JSGS、KBCS、KSSO、SMeO、WACS 等；TBCS 代表為本人與長庚郭玟伶醫師。議程架構由各學會代表進行自我與機構介紹。各學會以 3-4 分鐘概述組織概況與本國最新重點。TBCS 簡報乳癌專科認證體系、數位學習平台（乳 e 學院）雙語化、健保 P4P 品質政策與全國篩檢品質監測成果等亮點。SSO 蒐集各學會對未來合作項目（如聯合出版、跨國課程、年輕醫師交流、多中心研究）之意願。

SSO × TBCS 雙邊會議（Bilateral Meeting）

實質成果包含 TBCS 能見度強化，完整呈現台灣乳癌外科制度與數位政策優勢，並就聯合學術出版（ASO／SOI）、聯合 Webinar 與課程、年輕醫師交流（YDD/YDF）、跨國導師制（Mentorship）等形成初步共識。

(SSO 重要成員：SSO: Russell Berman, MD, FSSO; Cherif Boutros, MD; Ken Tanabe, MD, FSSO; Shishir Maithel, MD; Gabrielle van Ramshorst, MD, PhD; Tari King, MD; Chandrakanth Are, MD, MBA, FSSO, FRCS, FAC)

社交活動

Welcome Reception（3/4，HUB）、HUB Happy Hour（3/5）：促進與各國學會與專家之非正式交流，交換未來合作意向。

SSO President's Dinner（3/4，The El Chorro Lodge）：與 SSO 領導層面對面互動，建立信任與合作基礎。

(與哈佛大學 Kenneth Tanabe 教授-下任 SSO 主席與各國代表聚會)

心得及建議

本次參與 SSO 2026 年會，經由學術發表、Global Partner Leadership Summit 與雙邊會議等多層次互動，已達成本次出國之既定目標。會後將依本報告之合作方向，擬定時間表與分工，持續推動學術出版、聯合課程與人才交流，深化 TBCS 與 SSO 及各國學會之長期合作關係。此外成功於 SSO 年會 Global Partner Abstract Program 進行口頭報告，擴大台灣在乳癌轉譯研究之國際能見度。在 Global Partner Leadership Summit 建立合作方向，並於雙邊會議內聚焦落地項目，強化 TBCS 在制度建設（專科認證、雙語學習平台、P4P 與全國品質監測）之國際辨識度。中長期合作管道也期待能建立與多國學會之固定溝通窗口，有利於聯合學術、教育、年輕醫師培育與多中心研究。

附錄

Spatial Transcriptomic Profiling Uncovers Tumor Heterogeneity and Microenvironmental Features Associated with Lymph Node Metastasis in Invasive Lobular Carcinoma

Authors: Chih-Yi Hsu, MD[1], Nam Nhut Phan, PhD[2], Kate Hua, PhD[3], Chih-Sin Hsu, PhD[4], Wan-Chun Chang, MS[3], Bing-Xiu Guo, BS[3], Ling-Ming Tseng MD[5,6], Chi-Cheng Huang, MD, PhD[5,7]

[1]Department of Pathology, Taipei Veterans General Hospital, Taipei, Taiwan

[2]Greehey Children's Cancer Research Institute, University of Texas San Antonio, San Antonio, TX 78229

[3]Cancer and Immunology Research Center, National Yang Ming Chiao Tung University, Taipei, Taiwan

[4]Genomics Center for Clinical and Biotechnological Applications, Cancer and Immunology Research Center, National Yang Ming Chiao Tung University, Taipei, Taiwan

[5]Divison of Breast Surgery, Department of Surgery, Taipei Veterans General Hospital, Taiwan

[6]School of Medicine, College of Medicine, National Yang Ming Chiao Tung University, Taipei Taiwan

[7]Institute of Epidemiology and Preventive Medicine, College of Public Health, National Taiwan University, Taipei, Taiwan

Corresponding Author: Chi-Cheng Huang, MD, PhD

Division of Breast Surgery, Department of Surgery, Taipei Veterans General Hospital, Taipei, Taiwan; Email: chishenh74@gmail.com; Tel: 886-2-2871-2121

Ling-Ming Tseng, MD,

Division of Breast Surgery, Department ot Surgery, Taipei Veterans General Hospital, Taipei, Taiwan; Email: lmtseng87@gmail.com; Tel: 886-2-2871-2121

Abstract

Background: Invasive lobular carcinoma (ILC) is a clinically challenging, largely estrogen receptor-positive subtype characterized by dis-cohesive, single-file invasion and frequent lymph-node involvement. However, the spatial organization of ILC tumor ecosystems and the molecular features associated with nodal dissemination remain insufficiently defined.

Methods: We profiled a primary ILC and matched lymph-node metastasis using 10x Visium FFPE spatial transcriptomics (3,512 and 2,897 high-quality spots, respectively). Batch-corrected data were clustered and annotated. Differential expression and functional enrichment analyses were performed, with results integrated with histopathology.

Results: We identified 17 transcriptionally and spatially distinct clusters spanning tumor, stromal, and immune compartments. Consistent with the lobular phenotype, *CDH1* (E-cadherin) was significantly down-regulated in tumor cells, *EPCAM* was weak or absent across lobular regions. Comparing luminal lobular vs epithelial tumor cells, *HEPACAM2* was up-regulated while *TUSC3* was down-regulated, suggesting adhesion-linked migratory potential with altered glycoprotein handling. Spatial cell-type mapping revealed stromal remodeling in the primary tumor (cancer-associated fibroblasts [CAFs] 9.7%; matrix-remodeling cells 10.5%) with sparse immune infiltration, versus an immune-rich lymph node metastasis (macrophages 12.7%, B cells 11.1%, T cells 9.6%) and near-absence of CAFs.

Conclusions: Spatial transcriptomics delineates ILC as a luminal, adhesion-remodeled tumor that transitions from a fibroblast-rich primary niche to an immune-dominated metastatic node. The *CDH1*-low/*EPCAM*-low architecture, *HEPACAM2*/*TUSC3* axis, and pathway shifts nominate context-specific biomarkers and provide a framework to translate spatial insights into clinical ILC management.

Keywords: invasive lobular carcinoma; spatial transcriptomics; tumor microenvironment; lymph-node metastasis; HEPACAM2; TUSC3; CDH1; ECM/adhesion; immune niches

Introduction

Breast cancer is a heterogeneous disease composed of multiple subtypes with distinct molecular profiles, histological features, and clinical outcomes. Invasive lobular carcinoma (ILC) is the second most common subtype of breast cancer, accounting for approximately 5–15% of all invasive breast carcinomas, following invasive ductal carcinoma (IDC) [1-2]. Unlike IDC, which typically forms cohesive nests or duct-like structures, ILC is characterized by a diffuse, infiltrative growth pattern of small, dis-cohesive tumor cells, often arranged in single-file (Indian file) or solid/alveolar patterns within fibrous stroma [3]. This unique growth pattern makes ILC difficult to detect on mammography, frequently leading to larger tumor sizes at diagnosis and increased risk of distant metastasis to unusual sites, including the peritoneum, meninges, gastrointestinal tract, and ovaries [4].

The hallmark biological feature of ILC is the loss of E-cadherin, a cell adhesion molecule encoded by *CDH1*, which disrupts intercellular junctions and contributes to the dis-cohesive and infiltrative phenotype [5]. Most ILCs are hormone receptor, either estrogen receptor (ER) or progesterone receptor (PR), positive and human epidermal growth factor receptor II (HER2) negative, but their clinical behavior remains challenging to predict due to significant intratumor heterogeneity (ITH) and complex interactions within the tumor microenvironment (TME) [6-7]. Conventional transcriptomic approaches, such as bulk RNA sequencing and microarray, have provided valuable insights into ILC's molecular profile but fail to capture the spatial context of gene expression, which is critical for understanding how lobular carcinoma location may influence cancer and stromal cell function, interactions, and metastatic patterns [8-10].

Spatial transcriptomics (ST) is a revolutionary technology that preserves the spatial localization of cells while quantifying gene expression, bridging the gap between molecular profiling and histological morphology [11-13]. ST enables the decoding of ITH by revealing how genetically identical cells behave differently based on their position within the tumor, mapping the TME to identify cell-cell interactions, improving precision oncology by

identifying spatially distinct functional clusters, discovering novel subtypes and biomarkers, and integrating multi-omics data for clinical translation [14-15]. For ILC, which relies heavily on spatial context for its biological behavior and clinical presentation, ST offers a unique opportunity to unravel the molecular mechanisms underlying its diffuse growth and metastatic potential.

Despite the growing application of ST in breast cancer research, its use in ILC remains limited, and the spatial dynamics of tumor, stromal, and immune cells in primary and metastatic ILC are not fully characterized. In this study, we performed a ST analysis of primary ILC tissues and matched lymph node metastases using the 10x Genomics Visium platform [16]. Our goal was to investigate the spatial and transcriptional heterogeneity of ILC, characterize the TME, and identify molecular signatures associated with lymph node dissemination, with the aim of providing new insights for biomarker development and personalized therapeutic strategies.

Materials and Methods

Study Samples and Slide Preparation

Primary tumor and matched lymph node metastasis were collected from the same patient diagnosed with ILC at the Taipei Veterans General Hospital. All samples were obtained from institution's biobank, and the study was approved by the Institutional Review Board (IRB, No. 2025-01-012AC). H&E-stained sections were prepared from adjacent tissue blocks for histological confirmation of ILC and lymph node metastasis, with evaluation by a board-certified pathologist (CYH).

Total RNA was extracted from formalin-fixed paraffin-embedded (FFPE) tissue blocks using the RNeasy FFPE Kit (Qiagen, Hilden, Germany). Only samples demonstrating sufficient RNA quality, indicated by DV200 $\geq$30%, were eligible for subsequent analysis [17]. Qualified blocks were sectioned at 5 μm and mounted on SCHOTT NEXTERION 3-D Hydrogel Coating (H) slides (SCHOTT North America Inc., Rye Brook, NY). The sections were heat-fixed at 60°C for 2 hours using a C1000 Touch Thermal Cycler (Bio-Rad Laboratories, Inc., Hercules, CA). Following deparaffinization, the slides were stained with Hematoxylin (MilliporeSigma, Burlington, MA) and alcoholic Eosin Y (MilliporeSigma), and then cover slipped. Whole-slide images were captured at 10x magnification using an Olympus IX83 Motorized Inverted Fluorescence Microscope with Incubating System (Olympus Corporation, Tokyo, Japan).

Spatial Transcriptomic Sequencing

Spatial transcriptomic analysis was performed using the 10x Genomics Visium Spatial Gene Expression platform (10x Genomics, Pleasanton, CA, USA), following the manufacturer's standard protocol [18]. After coverslip removal and destaining, the sections were processed for spatial transcriptomic analysis using the Visium 2.0 CytAssist system to

position them over spots on Visium slides with a 6.5 mm^2 reaction area (CG000520 Rev B, 10x Genomics).

The cDNA libraries were prepared from the sections according to Visium CytAssist Spatial Gene Expression for FFPE User Guide (CG000495 Rev E, 10x Genomics) and sequenced on an Illumina NovaSeq 6000 (Illumina, San Diego, CA, USA) with paired-end reads. Space Ranger software (10x Genomics, version 3.0.0) was used for sequence alignment with the hg38 reference genome, tissue detection, fiducial detection, and barcode/unique molecular identifier (UMI) counting using whole slide images and sequencing (.fastq.gz) files as inputs. Space Ranger software further generated gene expression matrices, and map spatial barcodes to tissue coordinates. Output files included run summaries containing quality metrics, filtered feature-barcode matrices for spots overlayed with tissue sections, high-resolution images, and Loupe Browser files (.cloupe).

Data Processing and Analysis

Batch effects were corrected using the Harmony algorithm implemented in the Seurat package (v4.0.5) in R (v4.1.2) [19-20]. Dimensionality reduction was performed using principal component analysis (PCA) and uniform manifold approximation and projection (UMAP) [21]. Clustering analysis was performed using the Louvain algorithm to identify distinct spatial and transcriptional clusters [22].

Cell type annotation was conducted by integrating spatial gene expression data with known cell type markers: epithelial tumor cells (*EPCAM*, *KRT8*, *KRT18*), luminal tumor cells (*ESR1*, *PGR*, *GATA3*), cancer-associated fibroblasts (CAFs, represented by *ACTA2*, *FAP*, *PDGFRB*), immune cells (*CD3D*, *CD8A*, *CD68*, *MS4A1*), and adipocytes (*ADIPOQ*, *PLIN1*, *FABP4*). The Garnett1 automated cell type classification algorithm has been wrapped into Partek Flow (Illumina Inc., San Diego, CA) as the classification task. Cell type definition (marker) file used in the study is available as Supplementary Table 1 and trained a regression-based classifier [23]. Once a classifier (.rds) was completed, it was applied to classify future datasets from similar tissues.

Significant differentially expressed genes (DEGs) analysis between primary and metastatic tissues was performed using the Wilcoxon rank-sum test, with false discovery rate (FDR) correction < 0.05. Functional enrichment analysis of DEGs was conducted using the Database for Annotation, Visualization and Integrated Discovery (DAVID) v6.8, with enrichment in Kyoto Encyclopedia of Genes and Genomes (KEGG) pathways and Gene Ontology (GO) terms considered significant at FDR < 0.05 [24-26].

Results

Histopathological Features of ILC and Lymph Node Metastasis

Histopathological evaluation of H&E-stained sections confirmed the diagnosis of ILC in primary tumor tissue. ILC was characterized by small, bland, dis-cohesive tumor cells with round nuclei and scant cytoplasm, arranged in single-file or solid/ alveolar patterns within a fibrous, desmoplastic stroma (Figure 1, Top). Unlike IDC, no obvious duct-like structures were observed, and the tumor exhibited a diffuse, hypocellular appearance with scattered cells embedded in stroma, making it deceptively subtle. Lymph node metastasis from ILC showed effacement of normal nodal architecture, with tumor cells replacing the nodal parenchyma (Figure 1, Bottom). Metastatic tumor cells retained the dis-cohesive phenotype of primary ILC but often exhibited a more diffuse growth pattern, with occasional single-file infiltration and targetoid arrangements around residual nodal structures. Tumor cells were observed infiltrating close to or through the lymph node capsule, with evidence of extranodal extension into surrounding adipose tissue.

Spatial Transcriptomic Clustering and Cell Type Annotation

Spatial transcriptomic sequencing generated high-quality gene expression data from primary ILC and matched lymph node metastasis, with 3512 and 2897 high-quality spots (bins) per sample, respectively. ScType algorithm identified 17 distinct transcriptional clusters (8 in primary ILC and 9 in metastatic lymph node, ref. 27). UMAP visualization showed overlapping but distinct cell type distributions across both primary ILC and matched lymph node metastasis (Figure 2 Top and Bottom).

Further cell type annotation with Garnett1 revealed distinct clusters corresponding to epithelial tumor cells, luminal lobular tumor cells, CAFs, immune cells (T cells, B cells, macrophages), adipocytes, and matrix remodeling cells (Table 1, ref. 23). Primary ILC was dominated by epithelial tumor cells (24.3%) and luminal lobular tumor cells (14.3%), with a significant proportion of CAFs (9.7%), secretory CAFs (11.2%), and matrix remodeling cells (10.5%). In contrast, lymph node metastasis showed a dramatic reduction in epithelial tumor cells (0.2%), luminal lobular tumor cells (0.3%), CAFs (0.0%), and matrix remodeling cells (0.0%), with a significant increase in macrophages (12.7%), B cells (11.1%), T cells (9.6%), cytotoxic T cells (2.9%), regulatory T cells (4.0%), and adipocytes (10.3%). A large proportion of unknown cells (48.3%) was observed in lymph node metastases, likely reflecting the diffuse and heterogeneous nature of metastatic ILC (Table 1).

Key Molecular Signatures of ILC Tumor Cells

Tumor cell clusters (epithelial and luminal lobular) in primary and metastatic tissue expressed characteristic markers of ILC (Figure 3). *CDH1*, *MIA*, *KRT80*, *PTN*, *FDCSP*, *SMR3B*, *AK5*, *ID4*, *SFRP1*, *ITGB8*, *TGFBI*, *CNN1*, *NTN4*, *MCAM*, *NT5DC2*, *EGR3*, *TUSC3*, and *SGCE* were all down-regulated in ILC compared to epithelial tumor cells. Consistent with the histological hallmark of ILC, *CDH1* (encoding E-cadherin) was significantly downregulated in tumor cell clusters ($P=5e^{-47}$, FDR = $9e^{-43}$, fold change = -2.72). Down-regulatory features highlighted loss of epithelial program integrity, reduced extracellular matrix (ECM)-integrin/TGF-β signaling, lower neurotrophic/secretory signaling, and suppressed stress-response transcriptional activation. On the other hand, genes like *CXCL13*, *NPY2R*, *MYBL1*, *NCMAP*, *MSMB*, *UGT2B4*, *TRH*, and *PCDHGA5* aligned well with ILC biology and were all upregulated. These genes reflected a differentiated, hormone-driven, immune-modulated, and partially neuroendocrine-tuned biology.

DEGs analysis between luminal lobular tumor and epithelial tumor cells identified significant upregulation of *HEPACAM2* ($P = 5.41e^{-63}$, FDR = $9.74e^{-59}$, fold change = 2.62) and downregulation of *TUSC3* ($P = 3.94e^{-55}$, FDR = $3.54e^{-51}$, fold change = -2.17) in luminal

lobular tumor cells (Figure 4). *HEPACAM2* expression was positively correlated with luminal tumor cell identity ($\gamma = 0.28$), while *TUSC3* (a tumor suppressor) was downregulated in luminal lobular cells, suggesting enhanced migratory and invasive potential. *EPCAM* expression was weak or absent in lobular carcinoma regions, with limited expression detected only at the tumor periphery and in a small subset of metastatic spots (Supplementary Figure 1).

Tumor Microenvironment and Spatial Patterns

The TME of primary ILC was characterized by alternating patches of tumor cells embedded within fibroblast-rich stroma, with no sharp borders between tumor and non-tumor regions. In the primary tumor (Figure 5, Top), luminal lobular tumor cells form a large and cohesive cluster embedded within adipose-rich breast tissue and surrounded by abundant CAFs and matrix-remodeling stroma. Immune infiltrates, including T cells, B cells, and macrophages, were present but relatively sparse and localized to the tumor periphery. In contrast, the lymph-node metastasis (Figure 5, Bottom) exhibited a highly immune-enriched microenvironment, with dense populations of B cells, cytotoxic and regulatory T cells, and macrophages interwoven among smaller, fragmented clusters of metastatic tumor cells. Fibroblast populations were markedly depleted in the lymph-node sample, reflecting the stromal differences between breast tissue and lymphoid architecture. Together, these spatial maps highlighted the shift from a fibroblast-rich stromal niche in the primary tumor to an immune-dominated environment in the metastatic lymph node.

Functional Enrichment of Differentially Expressed Genes

Figure 6 shows functional enrichment analysis of DEGs between luminal lobular tumor and epithelial tumor cell clusters. Enrichment analyses converged on epithelial junction/adhesion and ECM/focal-adhesion programs, growth-factor/GPCR signaling (PI3K–AKT, MAPK, Ras/Rap1), hormone (estrogen) and immune/chemokine pathways, along with a neurotrophin/axon-guidance axis. GO terms with FDR < 0.05 concentrated in cell

adhesion/junction organization, cytoskeleton/migration, extracellular region, developmental processes, and neuron projection/myelination, consistent with known distinctions between invasive lobular carcinoma and epithelial/ductal phenotypes (Supplementary Table 2).

Discussion

In this study, we used spatial transcriptomics to characterize the spatial and transcriptional heterogeneity of primary ILC and matched lymph node metastasis, providing novel insights into the molecular mechanisms underlying ILC's unique biological behavior. Our findings confirmed that ST is a powerful tool for decoding ITH and TME interactions in ILC, overcoming the limitations of conventional transcriptomic approaches that lack spatial context [27-28].

The hallmark feature of ILC, loss of E-cadherin (*CDH1*), was consistently observed in tumor cell clusters, which disrupt intercellular adhesion and contribute to the dis-cohesive, infiltrative growth pattern [5]. This finding aligned with previous studies and confirmed the utility of ST for validating known ILC molecular signatures while providing spatial context [11-12]. Notably, we observed significant upregulation of *HEPACAM2* and downregulation of *TUSC3* in luminal lobular tumor cells. *HEPACAM2* is a cell adhesion molecule involved in cell migration and invasion, and its upregulation has been associated with increased metastatic potential in small cell lung cancer and canine mammary cells [29-30]. *TUSC3* is a tumor suppressor gene involved in protein glycosylation and endoplasmic reticulum stress response, and its downregulation has been linked to enhanced cell proliferation and invasion in multiple cancer types [31-34]. Together, these findings suggested that *HEPACAM2* and *TUSC3* may play critical roles in ILC's metastatic cascade, representing potential novel biomarkers and therapeutic targets.

Our analysis revealed dramatic differences in cell type distribution between primary ILC and lymph node metastasis. Primary tumor was dominated by tumor cells and stromal cells (CAFs, matrix remodeling cells), while matched lymph node metastasis showed a near-complete loss of stromal cells and a significant increase in immune cells (macrophages, B cells, T cells). This shift likely reflected the different microenvironmental pressures in lymph node metastasis, where tumor cells must evade immune surveillance to establish metastases. The increased in macrophages (12.7% in metastases vs. 0.9% in

primary tumors) was particularly notable, as M2-like macrophages (expressing CD163) are associated with immune suppression and metastatic progression [35-36]. The limited immune infiltrate in primary ILC (e.g., 1.1% T cells) might contribute to its immune-evasive phenotype, explaining why ILC tends to have lymph node metastasis due to its unique biological characteristics and growth patterns [37].

Although ILC generally elicits less desmoplastic response than IDC, the tumor-stroma interface remains a defining feature of primary ILC, in which stromal fibroblasts and matrix-remodeling cells often accompany the linear, single-file invasion pattern [38]. ILC spreads through tissue in a way that reflects interaction with and remodeling of the stromal microenvironment, which is consistent with the presence of CAFs and matrix-associated stromal cells. Igawa et al. described ameboid migration, perivascular infiltration, and lack of disturbance of background stroma, showing that ILC cells move through intact stromal architecture and use stromal structures during dissemination [39]. This supported the idea that stromal components, including fibroblasts, play a major role in primary tumor organization and progression. In contrast, lymph node metastasis from ILC demonstrated markedly different cellular organization and microenvironmental composition, with altered tumor cell morphology, increased density, and loss of the stromal context that characterizes the primary tumor site.

Spatial patterns of gene expression provided critical insights into ILC's growth and metastasis. Primary ILC exhibited diffuse, scattered tumor clusters embedded within fibroblast-rich stroma, with no sharp borders, consistent with its histological appearance and explaining its difficulty in detection [40]. Lymph node metastasis showed replacement of nodal parenchyma by tumor clusters, with mixed tumor-immune populations at interaction zones, suggesting dynamic crosstalk between tumor cells and the immune microenvironment. The admixture of tumor and adipocyte signals at capsular invasion regions highlighted potential metabolic interactions between tumor cells and axillary fat, which might support metastatic progression by providing energy and signaling molecules [41-42]. To sum up, primary ILC was dominated by tumor cells, and fibroblast-rich stroma, while immune cells were present but sparse. On the other hand, lymph node metastasis was strongly immune-rich, especially B cells, T cells, and macrophages. Tumor cells

appeared as smaller, fragmented islands and there were very few fibroblasts or adipose cells.

EPCAM, a commonly used epithelial marker in breast cancer, showed weak or absent expression in lobular carcinoma regions, with limited expression at the tumor periphery and in metastasis (Supplementary Figure 1). This finding was consistent with ILC's dis-cohesive phenotype [43]. EpCAM IHC expression frequently correlates with more aggressive tumor while its expression varies widely between cancers [44-45]. EpCAM expression in breast cancer depended on the histological subtype; lobular histology usually showed no or weak expression. Most IDC metastases were EpCAM positive and they frequently reflected the expression phenotype of the primary tumor [46].

Functional enrichment analysis and DEGs between luminal lobular and epithelial tumor cells indicated that genes down-regulated in ILC, including *CDH1*, *ITGB8*, *TGFBI*, *SFRP1*, *MCAM*, *CNN1*, *PTN*, and others, highlighting the loss of several pathways typically active in more cohesive or microenvironment-responsive epithelial tumors. Reduced *CDH1* expression reflected the hallmark loss of functional E-cadherin in ILC, while decreased levels of integrin/TGF-β–associated genes such as *ITGB8* and *TGFBI* suggest weakened cell–matrix adhesion and diminished stromal signaling [5, 47-49]. The suppression of motility-guidance and secretory genes (*PTN*, *NTN4*, *MIA*, *SMR3B*, *FDCSP*) further indicated a less paracrine-interactive phenotype, consistent with ILC's relatively "quiet," highly luminal transcriptional identity [5,50]. This pattern underscored that lobular tumors lack many ECM-activated, migratory, and paracrine programs present in other epithelial tumor types, reinforcing their distinct biology of dis-cohesive single-cell invasion and muted stromal engagement. Genes up-regulated in luminal lobular relative to epithelial tumor cells included *CXCL13*, *NPY2R*, *MYBL1*, *MSMB*, *UGT2B4*, *TRH*, and *PCDHGA5*. Elevated *CXCL13* suggested a more B-cell–skewed immune microenvironment, while increased *NPY2R* and *TRH* pointed toward enhanced neuroendocrine or neuromodulatory signaling within hormonally responsive luminal cells [39, 51-52]. Up-regulation of luminal secretory and steroid-metabolic genes (*MSMB*, *UGT2B4*) and the transcription factor *MYBL1* reinforced the highly differentiated, endocrine-dependent identity typical of ER-positive lobular tumors [53].

The adhesion/junction and ECM/focal adhesion signals (both KEGG and GO) aligned with the canonical difference: epithelial tumor cells retain strong cell-cell junctions (adherens/desmosome), whereas lobular tumors, defined by E-cadherin loss, shifted away from cohesive junctions and remodel interactions differently [54]. The neurotrophin/axon guidance and neuroendocrine flavor (KEGG: Neurotrophin signaling, Axon guidance; GO: axon/neuron projection terms) matched our identified lobular tumor up-regulated genes (*NPY2R* and *TRH*). Hormone (estrogen) and cytokine/chemokine terms supported a luminal, endocrine-responsive axis and immune contexture differences as *CXCL13* is the dominant chemokine recruiting B cells [55-56].

This study had several limitations. First, it was a preliminary analysis with a small sample size, and larger cohorts are needed to validate our findings. Second, we focused on lymph node metastases, and future studies should include distant metastases to better understand the full metastatic cascade. Third, we did not integrate multi-omics data (e.g., genomics, proteomics) with spatial transcriptomic data, which would provide a more comprehensive view of ILC's molecular landscape. Finally, functional studies are needed to confirm the roles of *HEPACAM2*, *TUSC3*, and other identified DEGs in ILC progression and metastasis. Despite these limitations, our findings advanced the understanding of ILC's spatial and molecular heterogeneity. The identification of *HEPACAM2* and *TUSC3* as key regulators of ILC metastasis opened new avenues for therapeutic development, while the limited role of *EPCAM* highlighted the need for ILC-specific biomarkers. Future studies should focus on validating these findings in larger cohorts, integrating multi-omics data, and translating spatial transcriptomic insights into clinical practice to improve outcomes for patients with ILC.

Conclusion

Spatial transcriptomic profiling revealed marked spatial and transcriptional heterogeneity in ILC, with distinct molecular and cellular features between primary tumors and lymph node metastasis. The loss of *CDH1*, upregulation of *HEPACAM2*, downregulation of *TUSC3*, and limited expression of *EPCAM* are key molecular signatures

of ILC, while shifts in cell type distribution (loss of stromal cells, increase in immune cells) characterize the metastatic microenvironment. Immune regulation pathways highlighted potential mechanisms of ILC progression and immune evasion. These findings demonstrated that spatial transcriptomics is a feasible and informative approach for characterizing ILC's complex architecture and provide valuable insights for the development of improved biomarkers and personalized therapeutic strategies.

Acknowledgements

This study was supported by NSTC-114-2314-B-075-047- from National Science and Technology Council and Taipei Veterans General Hospital (grant number: V113E-004-3, V114E-002-3 and V115E-003-3) and Melissa Lee Cancer Foundation (project number: MLCF_V113_B11305, MLCF_V114_B11404, MLCF_V115_B11501). The authors acknowledge the spatial transcriptomic analysis (Visium 2.0 CytAssist) provided by the National Genomics Center for Clinical and Biotechnological Applications of the Cancer and Immunology Research Center (National Yang Ming Chiao Tung University). The National Core Facility for Biopharmaceuticals (NCFB), National Science and Technology Council (NSTC). The authors would like to thank Mr. Kuan-Hao Hsu and Mr. Ying-Yuan Chen of Genetech Biotech, Taipei, Taiwan and Dr. Morris Chang for their kind assistance during the study.

Conflicts of Interest

The author declares no conflicts of interest.

References

1. McCart Reed AE, Kalinowski L, Simpson PT, Lakhani SR. Invasive lobular carcinoma of the breast: the increasing importance of this special subtype. Breast Cancer Res. 2021;23:6.

2. Chen BF, Tsai YF, Lien PJ, Lin YS, Feng CJ, Chen YJ, Cheng HF, Tseng LM, Huang CC. Clinical characteristics and treatment outcomes of invasive ductal and lobular carcinoma: analyses of 54,832 taiwan cancer registry index cases. Breast Cancer Res Treat. 2023;201:547-560.

3. McCart Reed AE, Kutasovic JR, Lakhani SR, Simpson PT. Invasive lobular carcinoma of the breast: morphology, biomarkers and 'omics. Breast Cancer Res. 2015;17:12.

4. Brem RF, Ioffe M, Rapelyea JA, Yost KG, Weigert JM, Bertrand ML, Stern LH. Invasive lobular carcinoma: detection with mammography, sonography, MRI, and breast-specific gamma imaging. AJR Am J Roentgenol. 2009;192:379-83.

5. Dopeso H, Gazzo AM, Derakhshan F, Brown DN, Selenica P, Jalali S, Da Cruz Paula A, Marra A, da Silva EM, Basili T, Gusain L, Colon-Cartagena L, Bhaloo SI, Green H, Vanderbilt C, Oesterreich S, Grabenstetter A, Kuba MG, Ross D, Giri D, Wen HY, Zhang H, Brogi E, Weigelt B, Pareja F, Reis-Filho JS. Genomic and epigenomic basis of breast invasive lobular carcinomas lacking CDH1 genetic alterations. NPJ Precis Oncol. 2024;8:33.

6. Pramod N, Nigam A, Basree M, Mawalkar R, Mehra S, Shinde N, Tozbikian G, Williams N, Majumder S, Ramaswamy B. Comprehensive Review of Molecular Mechanisms and Clinical Features of Invasive Lobular Cancer. Oncologist. 2021;26:e943-e953.

7. Corso G, Shen S, Criscitiello C, Mukhtar R, Gamble L, Rocco EG, Pesapane F, Nicosia L, Jhaveri K, Salimbeni BT, Massari G, Meduri E, De Scalzi AM, Concardi A, Magnoni F, Mamtani A, Pareja F, Leonardi MC, Sacchini V, Bogani G, Vecchia C, Presti D, Colleoni MA, Veronesi P, Robson ME. Invasive lobular carcinoma: Strategies and perspectives from the

lobular breast cancer research group. Cancer Treat Rev. 2025;140:103001.

8. Ozawa N, Takeyama E, Sakai H, Katayama A, Onishi M, Kizawa R, Matsunaga Y, Nozawa K, Umezaki N, Mitsueda R, Tanabe K, Sekine C, Golshan M, Rakha EA, Horiguchi J, Kurozumi S. Molecular and Biological Features of Invasive Lobular Carcinoma: Toward New Treatment Strategies. Ann Surg Oncol. 2026;33:146-158.

9. Michaut M, Chin SF, Majewski I, Severson TM, Bismeijer T, de Koning L, Peeters JK, Schouten PC, Rueda OM, Bosma AJ, Tarrant F, Fan Y, He B, Xue Z, Mittempergher L, Kluin RJ, Heijmans J, Snel M, Pereira B, Schlicker A, Provenzano E, Ali HR, Gaber A, O'Hurley G, Lehn S, Muris JJ, Wesseling J, Kay E, Sammut SJ, Bardwell HA, Barbet AS, Bard F, Lecerf C, O'Connor DP, Vis DJ, Benes CH, McDermott U, Garnett MJ, Simon IM, Jirström K, Dubois T, Linn SC, Gallagher WM, Wessels LF, Caldas C, Bernards R. Integration of genomic, transcriptomic and proteomic data identifies two biologically distinct subtypes of invasive lobular breast cancer. Sci Rep. 2016;6:18517.

10. Turashvili G, Bouchal J, Baumforth K, Wei W, Dziechciarkova M, Ehrmann J, Klein J, Fridman E, Skarda J, Srovnal J, Hajduch M, Murray P, Kolar Z. Novel markers for differentiation of lobular and ductal invasive breast carcinomas by laser microdissection and microarray analysis. BMC Cancer. 2007 Mar;7:55.

11. Serra M, Rediti M, Collet L, Lifrange F, Venet D, Occelli N, Papagiannis A, Vincent D, Rouas G, Larsimont D, Vikkula M, Duhoux FP, Rothé F, Sotiriou C. Spatial transcriptomics reveals tumor microenvironment-driven subtypes of invasive lobular carcinoma. Proc Natl Acad Sci U S A. 2026;123:e2517567123.

12. An J, Lu Y, Chen Y, Chen Y, Zhou Z, Chen J, Peng C, Huang R, Peng F. Spatial transcriptomics in breast cancer: providing insight into tumor heterogeneity and promoting individualized therapy. Front Immunol. 2024;15:1499301.

13. Stuart T, Butler A, Hoffman P, Hafemeister C, Papalexi E, Mauck WM 3rd, Hao Y, Stoeckius M, Smibert P, Satija R. Comprehensive Integration of Single-Cell Data. Cell. 2019;177:1888-1902.e21.

14. Pattabiram S, Gangadaran P, Dhayalan S, Chatterjee G, Reyaz D, Prakash K, Arun R, Rajendran RL, Ahn BC, Aruljothi KN. Decoding the Tumor Microenvironment: Insights and New Targets from Single-Cell Sequencing and Spatial Transcriptomics. Curr Issues Mol Biol. 2025;47:730.

15. Shi W, Zhang Z, Xu X, Tian Y, Feng L, Huang X, Du Y, Li Z. Single-cell and spatial transcriptomics integration: new frontiers in tumor microenvironment and cellular communication. Front Immunol. 2025;16:1649468.

16. Janesick A, Shelansky R, Gottscho AD, Wagner F, Williams SR, Rouault M, Beliakoff G, Morrison CA, Oliveira MF, Sicherman JT, Kohlway A, Abousoud J, Drennon TY, Mohabbat SH; 10x Development Teams; Taylor SEB. High resolution mapping of the tumor microenvironment using integrated single-cell, spatial and in situ analysis. Nat Commun. 2023;14:8353.

17. 10x Genomics. Visium CytAssist Spatial Gene Expression for FFPE – Deparaffinization, H&E Staining, Imaging & Decrosslinking (Demonstrated Protocol, CG000520, Rev A). 10x Genomics, Pleasanton, CA. Available at: https://assets.ctfassets.net/an68im79xiti/4Rdssn2Po0XlJp2xcBkBbt/8f7d4220689e3f3270b23412b4dac182/CG000520_Demonstrated_Protocol_VisiumCytAssist_Deparaffin_H_E_Rev A.pdf.

18. 10x Genomics. Visium CytAssist Instrument User Guide with Readiness Test (Document CG000542, Rev K). 10x Genomics, Pleasanton, CA; September 2025. Available at: https://cdn.10xgenomics.com/image/upload/v1759179831/support-documents/CG000542_VisiumCytAssist_Instrument_UserGuide_RevK.pdf.

19. Hao Y, Hao S, Andersen-Nissen E, Mauck WM 3rd, Zheng S, Butler A, Lee MJ, Wilk AJ, Darby C, Zager M, Hoffman P, Stoeckius M, Papalexi E, Mimitou EP, Jain J, Srivastava A, Stuart T, Fleming LM, Yeung B, Rogers AJ, McElrath JM, Blish CA, Gottardo R, Smibert P, Satija R. Integrated analysis of multimodal single-cell data. Cell. 2021;184:3573-3587.e29.

20. R Core Team (2021). R: A language and environment for statistical computing. R Foundation for Statistical Computing, Vienna, Austria. https://www.R-project.org/.

21. Giraldo NA, Berry S, Becht E, Ates D, Schenk KM, Engle EL, Green B, Nguyen P, Soni A, Stein JE, Succaria F, Ogurtsova A, Xu H, Gottardo R, Anders RA, Lipson EJ, Danilova L, Baras AS, Taube JM. Spatial UMAP and Image Cytometry for Topographic Immuno-oncology Biomarker Discovery. Cancer Immunol Res. 2021;9:1262-1269.

22. Seth S, Mallik S, Bhadra T, Zhao Z. Dimensionality Reduction and Louvain Agglomerative Hierarchical Clustering for Cluster-Specified Frequent Biomarker Discovery in Single-Cell Sequencing Data. Front Genet. 2022;13:828479.

23. Pliner HA, Shendure J, Trapnell C. Supervised classification enables rapid annotation of cell atlases. Nat Methods. 2019;16:983-986.

24. Sherman BT, Hao M, Qiu J, Jiao X, Baseler MW, Lane HC, Imamichi T, Chang W. DAVID: a web server for functional enrichment analysis and functional annotation of gene lists (2021 update). Nucleic Acids Res. 2022;50:W216-W221.

25. Kanehisa M, Furumichi M, Sato Y, Matsuura Y, Ishiguro-Watanabe M. KEGG: biological systems database as a model of the real world. Nucleic Acids Res. 2025;53:D672-D677.

26. Ashburner M, Ball CA, Blake JA, Botstein D, Butler H, Cherry JM, Davis AP, Dolinski K, Dwight SS, Eppig JT, Harris MA, Hill DP, Issel-Tarver L, Kasarskis A, Lewis S, Matese JC, Richardson JE, Ringwald M, Rubin GM, Sherlock G. Gene ontology: tool for the unification of biology. The Gene Ontology Consortium. Nat Genet. 2000;25:25-9.

27. Nader K, Tasci M, Ianevski A, Erickson A, Verschuren EW, Aittokallio T, Miihkinen M. ScType enables fast and accurate cell type identification from spatial transcriptomics data. Bioinformatics. 2024;40:btae426.

28. Xu W, Lu J, Zhang H, Ye D. Decoding the tumor microenvironment: insights into immunotherapy and beyond. J Natl Cancer Cent. 2025;5:426-428.

29. Liu Y, Dai Y, Wang L. Spatial omics at the forefront: emerging technologies, analytical innovations, and clinical applications. Cancer Cell. 2026;44:24-49.

30. Klopfleisch R, Klose P, da Costa A, Brunnberg L, Gruber AD. HEPACAM1 and 2 are differentially regulated in canine mammary adenomas and carcinomas and its lymph node metastases. BMC Vet Res. 2010;6:15.

31. McColl KS, Ajay A, Wang H, Wildey GM, Yoon S, Grubb B, Kopp SR, Joseph PL, Saviana M, Romano G, Nana-Sinkam P, Peacock CD, Yun Z, Mneimneh W, Lam M, Miyagi M, Kao HY, Dowlati A. Identification of HEPACAM2 as a novel and specific marker of small cell carcinoma. Cancer. 2025;131:e35557.

32. Sun F, Jie Q, Li Q, Wei Y, Li H, Yue X, Ma Y. TUSC3 inhibits cell proliferation and invasion in cervical squamous cell carcinoma via suppression of the AKT signalling pathway. J Cell Mol Med. 2022;26:1629-1642.

33. Deng R, Lu X, Hong C, Cai R, Wang P, Xiong L, Wang X, Chen Q, Lin J. Downregulation of TUSC3 promotes EMT and hepatocellular carcinoma progression through LIPC/AKT axis. J Transl Med. 2022;20:485.

34. Fan X, Zhang X, Shen J, Zhao H, Yu X, Chen Y, Zhuang Z, Deng X, Feng H, Wang Y, Peng L. Decreased TUSC3 Promotes Pancreatic Cancer Proliferation, Invasion and Metastasis. PLoS One. 2016;11:e0149028.

35. Horak P, Tomasich E, Vaňhara P, Kratochvílová K, Anees M, Marhold M, Lemberger CE, Gerschpacher M, Horvat R, Sibilia M, Pils D, Krainer M. TUSC3 loss alters the ER stress response and accelerates prostate cancer growth in vivo. Sci Rep. 2014;4:3739.

36. Ni C, Yang L, Xu Q, Yuan H, Wang W, Xia W, Gong D, Zhang W, Yu K. CD68- and CD163-positive tumor infiltrating macrophages in non-metastatic breast cancer: a retrospective study and meta-analysis. J Cancer. 2019;10:4463-4472.

37. Medrek C, Pontén F, Jirström K, Leandersson K. The presence of tumor associated macrophages in tumor stroma as a prognostic marker for breast cancer patients. BMC Cancer. 2012;12:306.

38. Fernández B, Paish EC, Green AR, Lee AH, Macmillan RD, Ellis IO, Rakha EA. Lymph-

node metastases in invasive lobular carcinoma are different from those in ductal carcinoma of the breast. J Clin Pathol. 2011;64:995-1000.

39. Yu B, Yan L, Wang H, Yang J, Yang J. Invasive lobular carcinoma of the breast: metastatic patterns and treatment modalities-a review. Front Oncol. 2025;15:1631670.

40. Igawa A, Mizukami H, Kudoh K, Takeuchi Y, Sasaki T, Pan X, Hakamada K. Perivascular infiltration reflects subclinical lymph node metastasis in invasive lobular carcinoma. Virchows Arch. 2022;481:533-543.

41. Serra M, Papagiannis A, Rediti M, Lifrange F, Occelli N, Collet L, Vincent D, Rouas G, Fimereli D, Craciun L, Larsimont D, Venet D, Duhoux F, Vikkula M, Rothé F, Sotiriou C. Abstract 5066: Integrating spatial and single cell transcriptomics to identify and characterise biologically driven subgroups in invasive lobular carcinoma. Cancer Res. 2024;84(6_Suppl):5066.

42. Serra M, Rediti M, Collet L, Lifrange,F Venet D, Occelli N, Vincent D, Rouas G, Larsimont D, Vikkula M, Duhoux FP, Rothé F, Sotiriou C. Abstract PS18-01: Spatial Transcriptomics-Derived Classification of Invasive Lobular Carcinoma: Associations with Clinical, Genomic Characteristics, and Prognosis. Clin Cancer Res. 2025;31 (12_Supplement):PS18–01.

43. Serra M, Collet L, Rediti M, Lifrange F, Venet D, Occelli N, Vincent D, Rouas G, Larsimont D, Craciun L, Wang X, Gacquer D, Vikkula M, Duhoux FP, Rothé F, Sotiriou C. 1726P Investigating adipocytes–tumor cells interaction and its effect on disease progression in lobular breast cancer with spatial transcriptomics. Ann Oncol. 2022;33(Suppl 7):S1326.

44. Spizzo G, Fong D, Wurm M, Ensinger C, Obrist P, Hofer C, Mazzoleni G, Gastl G, Went P. EpCAM expression in primary tumour tissues and metastases: an immunohistochemical analysis. J Clin Pathol. 2011;64:415-20.

45. Aslemarz A, Fagotto-Kaufmann M, Ruppel A, Fagotto-Kaufmann C, Balland M, Lasko P, Fagotto F. An EpCAM/Trop2 mechanostat differentially regulates collective behaviour of human carcinoma cells. EMBO J. 2025;44:75-106.

46. Fagotto F, Aslemarz A. EpCAM cellular functions in adhesion and migration, and potential impact on invasion: A critical review. Biochim Biophys Acta Rev Cancer. 2020;1874:188436.

47. Munger JS, Sheppard D. Cross talk among TGF-β signaling pathways, integrins, and the extracellular matrix. Cold Spring Harb Perspect Biol. 2011;3:a005017.

48. Margadant C, Sonnenberg A. Integrin-TGF-beta crosstalk in fibrosis, cancer and wound healing. EMBO Rep. 2010;11:97-105.

49. Chen PY, Qin L, Simons M. TGFβ signaling pathways in human health and disease. Front Mol Biosci. 2023;10:1113061.

50. Uchida S, Sugino T. Insights into E-Cadherin Impairment in CDH1-Unaltered Invasive Lobular Carcinoma: A Comprehensive Bioinformatic Study. Int J Mol Sci. 2024;25:8961.

51. Ciriello G, Gatza ML, Beck AH, Wilkerson MD, Rhie SK, Pastore A, Zhang H, McLellan M, Yau C, Kandoth C, Bowlby R, Shen H, Hayat S, Fieldhouse R, Lester SC, Tse GM, Factor RE, Collins LC, Allison KH, Chen YY, Jensen K, Johnson NB, Oesterreich S, Mills GB, Cherniack AD, Robertson G, Benz C, Sander C, Laird PW, Hoadley KA, King TA; TCGA Research Network; Perou CM. Comprehensive Molecular Portraits of Invasive Lobular Breast Cancer. Cell. 2015;163:506-19.

52. Mouabbi JA, Hassan A, Lim B, Hortobagyi GN, Tripathy D, Layman RM. Invasive lobular carcinoma: an understudied emergent subtype of breast cancer. Breast Cancer Res Treat. 2022;193:253-264.

53. Sun C, Huo D, Southard C, Nemesure B, Hennis A, Cristina Leske M, Wu SY, Witonsky DB, Olopade OI, Di Rienzo A. A signature of balancing selection in the region upstream to the human UGT2B4 gene and implications for breast cancer risk. Hum Genet. 2011;130:767-75.

54. Rübsam M, Broussard JA, Wickström SA, Nekrasova O, Green KJ, Niessen CM. Adherens Junctions and Desmosomes Coordinate Mechanics and Signaling to Orchestrate

Tissue Morphogenesis and Function: An Evolutionary Perspective. Cold Spring Harb Perspect Biol. 2018;10:a029207.

55. Kowarik MC, Cepok S, Sellner J, Grummel V, Weber MS, Korn T, Berthele A, Hemmer B. CXCL13 is the major determinant for B cell recruitment to the CSF during neuroinflammation. J Neuroinflammation. 2012;9:93.

56. Rubio AJ, Porter T, Zhong X. Duality of B Cell-CXCL13 Axis in Tumor Immunology. Front Immunol. 2020;11:521110.

Tables

Table 1. Cell type distributions in primary invasive lobular carcinoma (ILC) and lymph node metastasis using the Garnett1 classifier [23].

Cell type	Primary ILC		lymph node metastasis	
	Count	Percent	Count	Percent
Adipose cells	196	5.60%	299	10.30%
B cells	72	2.10%	323	11.10%
Cancer-associated fibroblasts (CAFs)	340	9.70%	1	0.00%
Cytotoxic T cells	1	0.00%	83	2.90%
Epithelial tumor cells	853	24.30%	5	0.20%
Luminal lobular tumor cells	503	14.30%	10	0.30%
M2 like macrophages	—	—	3	0.10%
Macrophages	33	0.90%	367	12.70%
Matrix remodeling	368	10.50%	1	0.00%
Proliferative tumor cells	104	3.00%	9	0.30%
Regulatory T cells	—	—	115	4.00%
Secretory CAF	394	11.20%	4	0.10%
T Cells	40	1.10%	278	9.60%
Unknown	608	17.30%	1399	48.30%

Figures Legends

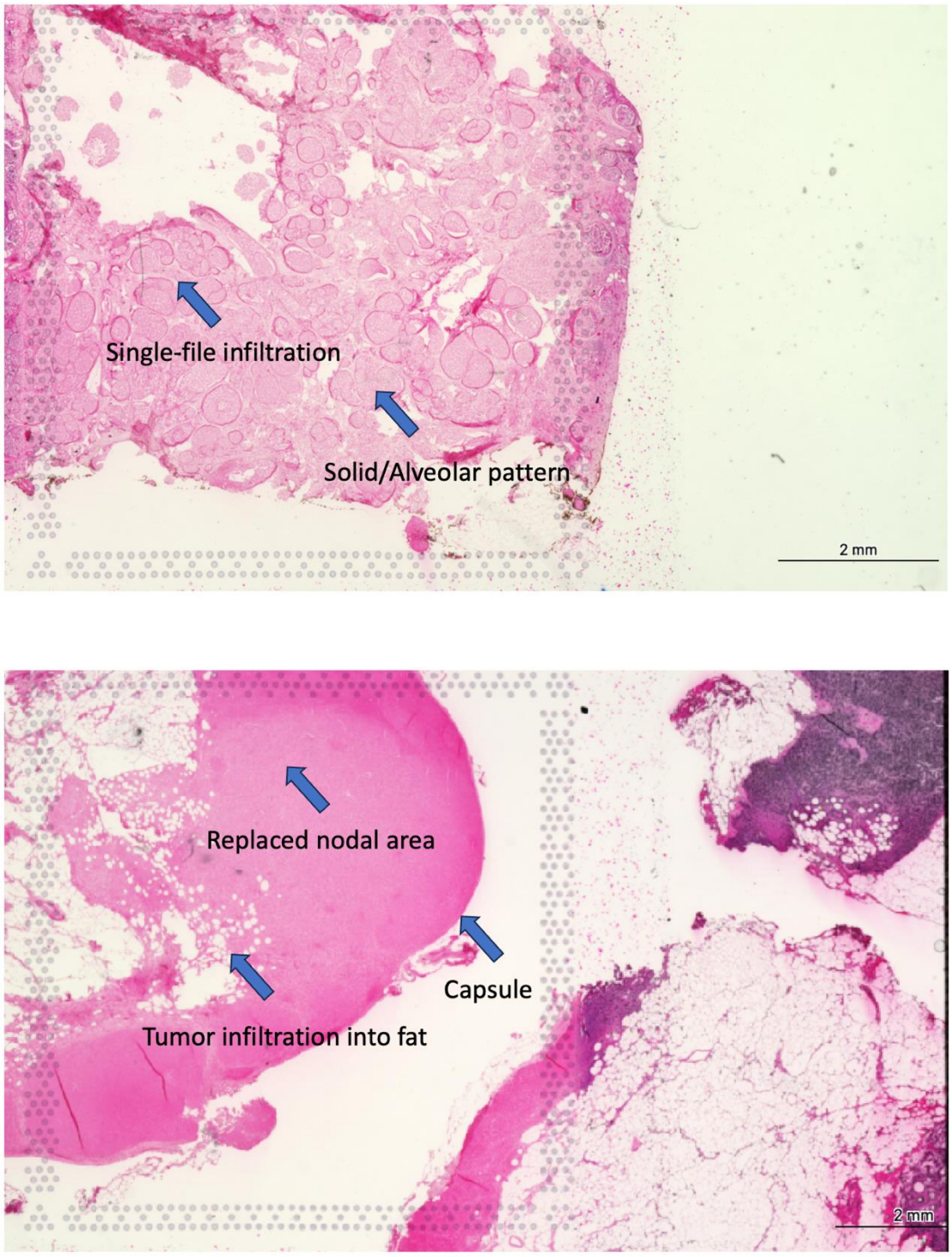

Figure 1. Histopathological features of primary invasive lobular carcinoma (ILC) and lymph node metastasis. (Top) ILC showing small, dis-cohesive tumor cells arranged in single-file, solid or alveolar patterns within fibrous stroma (H&E staining, ×200). (Bottom) Lymph node metastasis from ILC showing effacement of nodal architecture by diffuse, dis-cohesive

tumor cells with adipose tissue and capsular involvement (H&E staining, ×100).

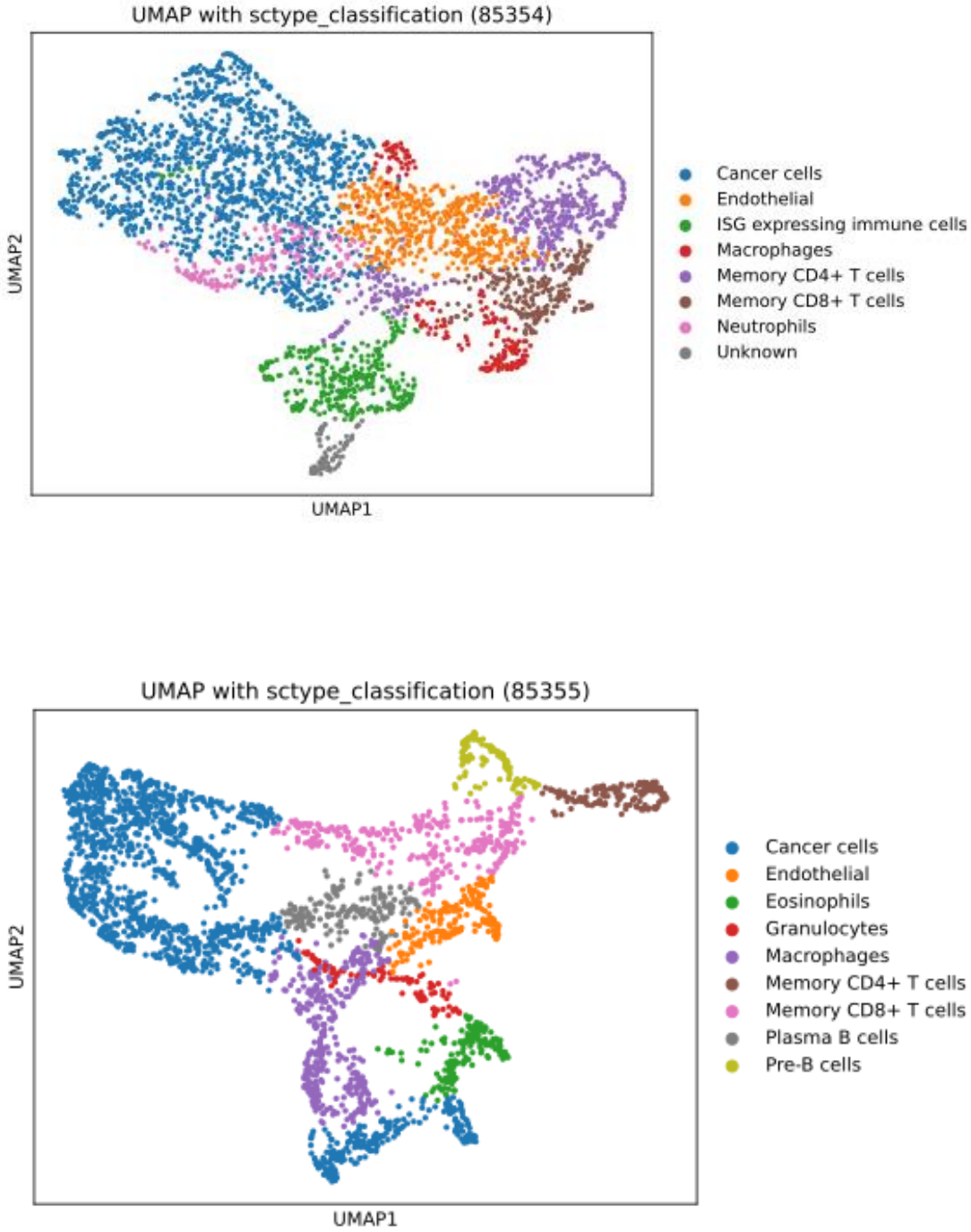

Figure 2. Spatial transcriptomic clustering with uniform manifold approximation and projection (UMAP) visualization of primary invasive lobular carcinoma (ILC, Top) and matched lymph node metastasis (Bottom). Using scType classification [27], 8 and 9 clusters (cell types) were identified within the primary tumor and matched lymph node, respectively.

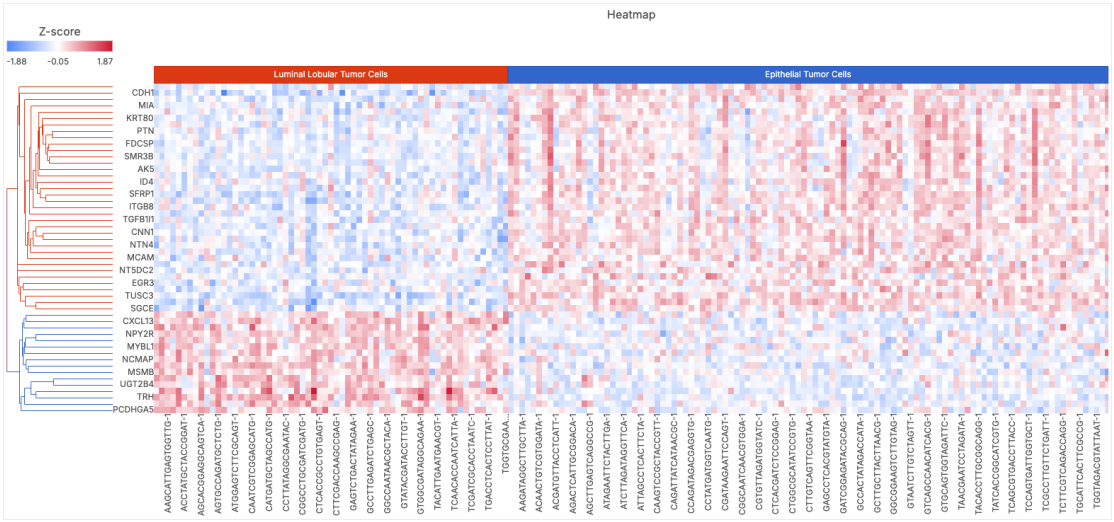

Figure 3. Marker gene expression in luminal lobular tumor cells (left) and epithelial tumor cells (right). Heatmap shows expression of key marker genes in epithelial and luminal lobular tumor clusters from primary and metastatic tissues. Z-scores indicate relative expression levels.

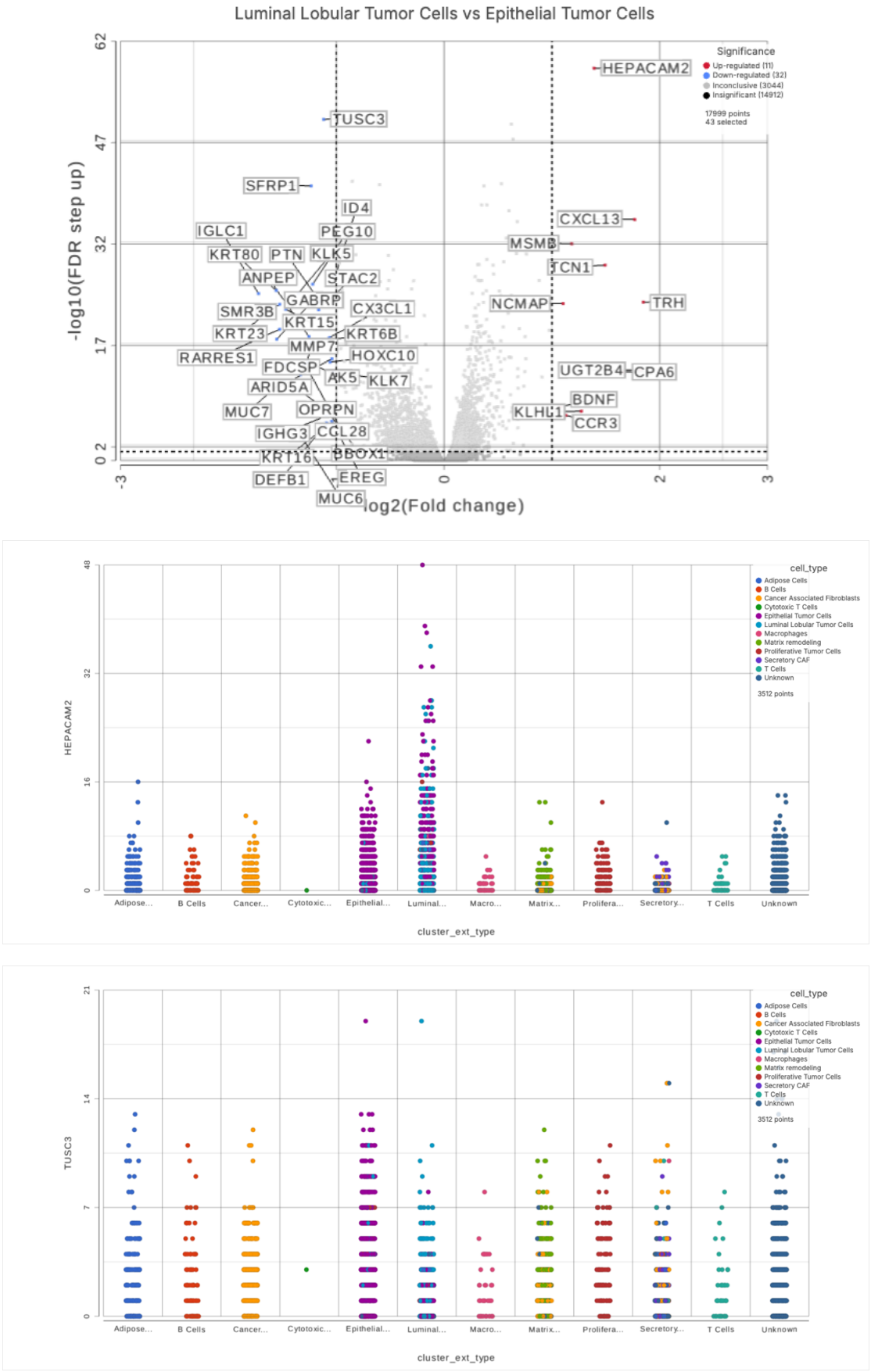

Figure 4. Differentially expressed genes (DEGs) between luminal lobular tumor and epithelial tumor cells. Volcano plot (Top) shows DEGs, with *HEPACAM2* (upregulated) and

TUSC3 (downregulated) highlighted. Dot plots (Middle and Bottom) show expression of *HEPACAM2* and *TUSC3* across cell types.

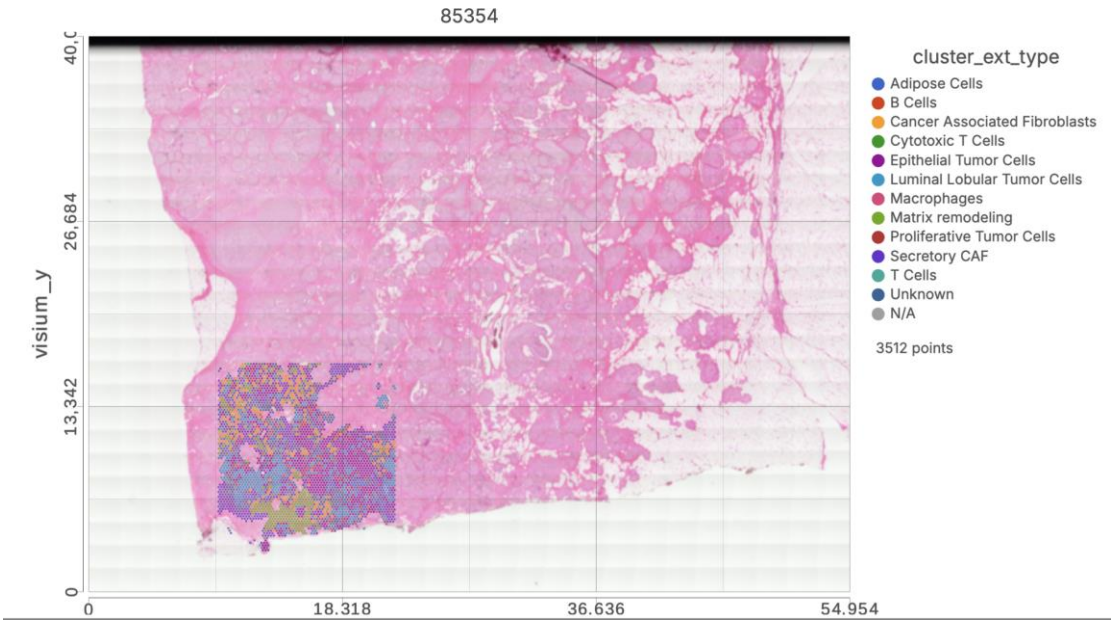
85354
visium_y
0
13,342
26,684
0
18.318
36.636
54.954
cluster_ext_type
Adipose Cells
B Cells
Cancer Associated Fibroblasts
Cytotoxic T Cells
Epithelial Tumor Cells
Luminal Lobular Tumor Cells
Macrophages
Matrix remodeling
Proliferative Tumor Cells
Secretory CAF
T Cells
Unknown
N/A
3512 points

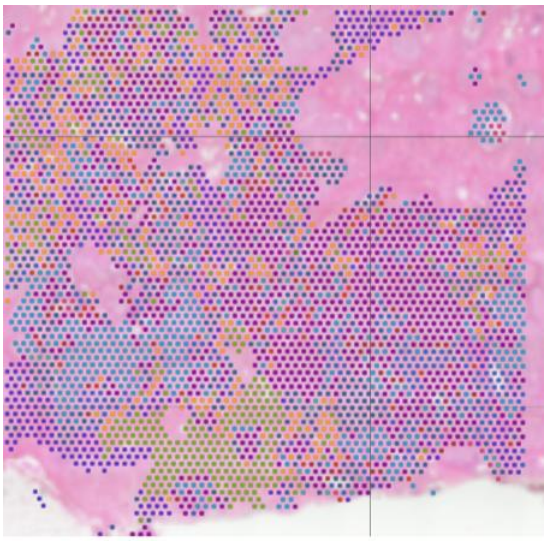

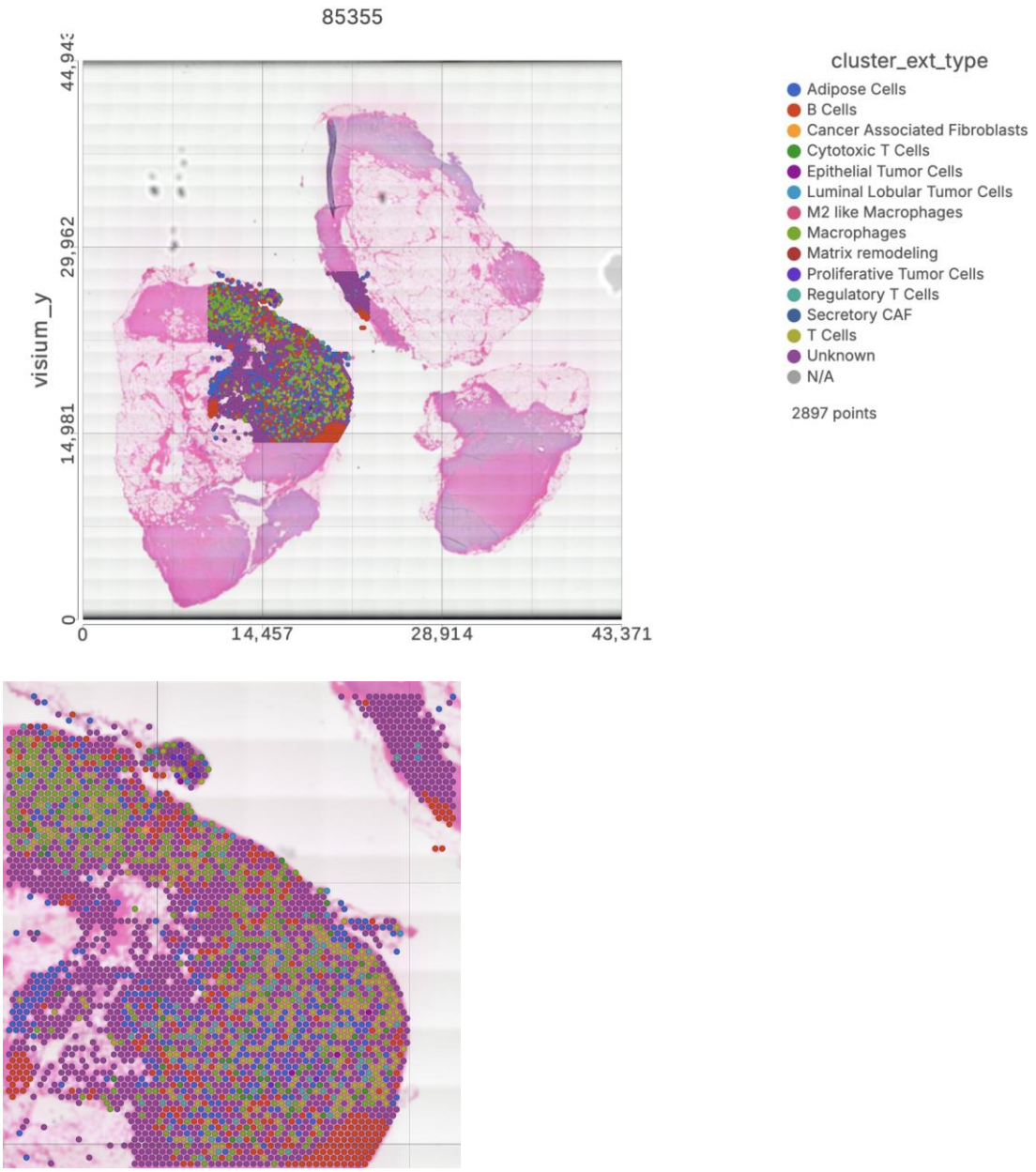

Figure 5. Spatial cell-type architecture in the primary invasive lobular carcinoma (ILC, Top) and matched lymph-node metastasis (Bottom). In primary ILC, luminal lobular tumor cells (purple) form a large, cohesive cluster embedded within breast stroma that is rich in cancer-associated fibroblasts (CAFs, yellow) and matrix-remodeling fibroblasts (olive), adjacent to extensive adipose tissue (blue). Immune infiltrates, including T cells (dark green), cytotoxic T cells (bright green), B cells (orange), and macrophages (red), are present but relatively sparse and peripheral. In lymph node metastasis, tumor cells (luminal lobular, purple; epithelial tumor cells, light blue) appear as smaller, fragmented clusters interwoven with dense lymphoid populations, including abundant B cells (orange), T cells (dark green), cytotoxic T cells (bright green), regulatory T cells (lime), and

macrophages/M2-like macrophages (red/dark red). Fibroblast populations (CAF, yellow; matrix-remodeling, olive; secretory CAF, pink) are markedly reduced, and adipose cells (blue) are minimal, reflecting the stromal differences between breast tissue and lymphoid architecture.

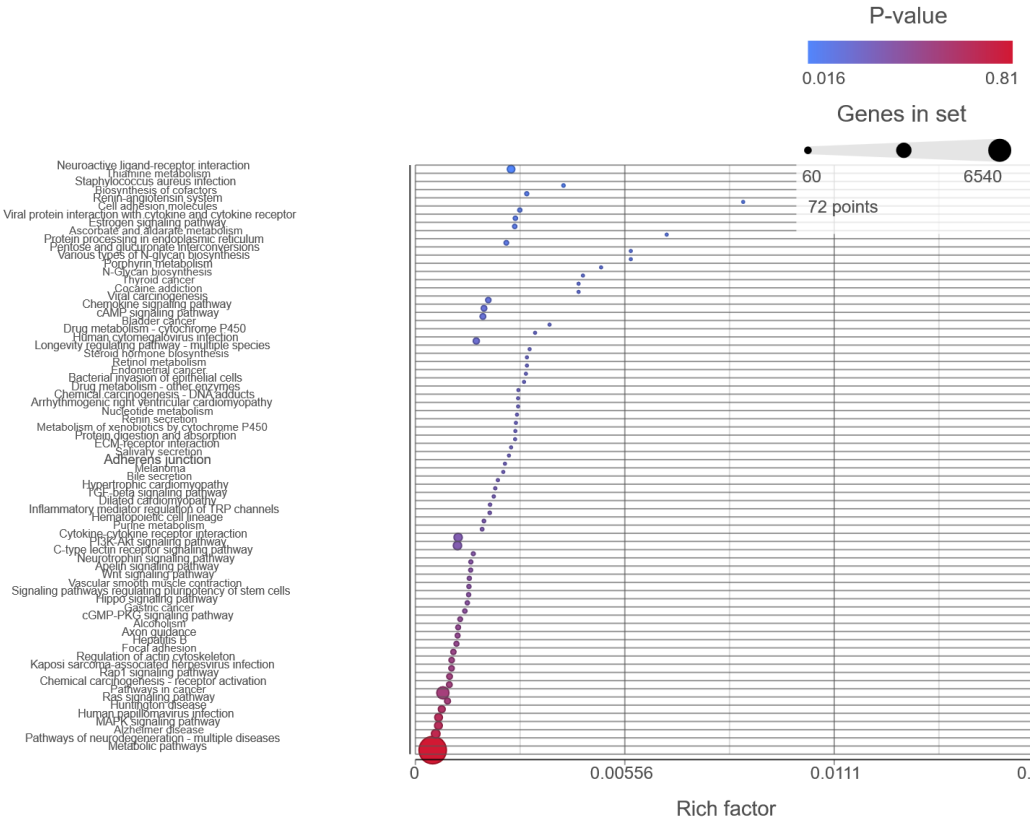

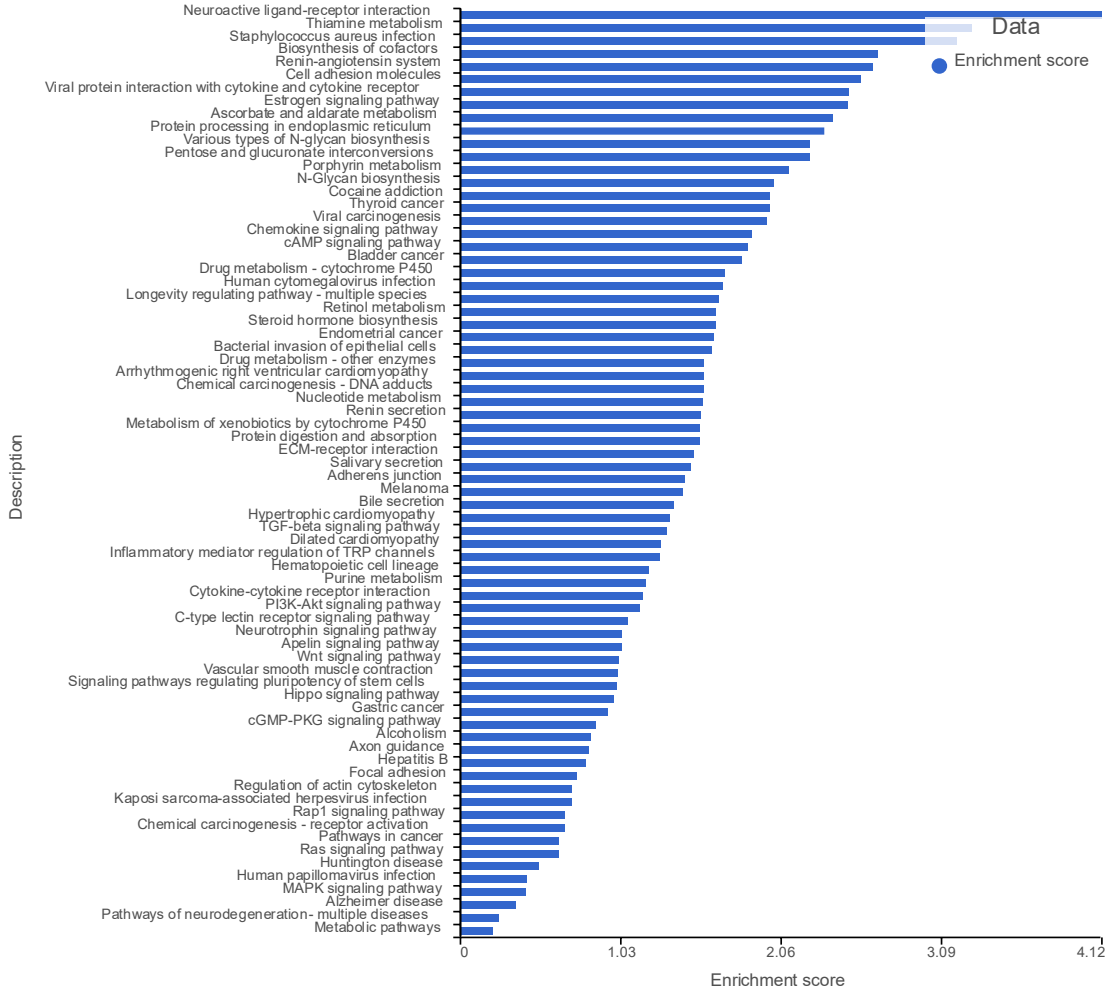

Figure 6. Functional enrichment of differentially expressed genes (DEGs). Bar plot shows significantly enriched Kyoto Encyclopedia of Genes and Genomes (KEGG) pathways and Gene Ontology (GO) terms in DEGs between luminal lobular tumor and epithelial tumor cells, with enrichment scores and P-values indicated [25-26].